Research Article

Tianyou Wang, Zhiying Li*, Jie Wang, Changrong Li, Zeyun Zeng, and Fulong Wei

Effect of different isothermal times on the microstructure and mechanical properties of high-strength rebar

https://doi.org/10.1515/htmp-2022-0266
received September 14, 2022; accepted December 18, 2022

Abstract: High-strength rebar plays a supporting role in large engineering structures due to its excellent performance. In this study, the effect of different isothermal time treatments (30, 60, 100, and 200 s) at 650°C on the microstructure transformation and mechanical properties of rebars was investigated. The hot-rolling process was simulated by Gleeble-3800 thermal simulator. The microstructure, precipitates, and mechanical properties of high-strength rebar were characterized by scanning electron microscopy, transmission electron microscopy (TEM), and a universal tensile test machine. Results show that when the isothermal time increased from 30 to 200 s, the ferrite grain size decreased from 10.632 to 8.326 μm, and the pearlite lamellar spacing was refined from 0.230 to 0.142 μm. The TEM confirmed that when the isothermal time increased from 30 to 200 s, the nanoscale (Nb, V, and Ti) C precipitates were uniformly distributed in the ferrite matrix and grain boundary, and the size of precipitates decreased from 34.014 to 29.916 nm; thus, the tensile strength increased from 752.477 to 780.713 MPa, and the yield strength increased from 574.714 to 621.434 MPa.

Keywords: high-strength rebar, isothermal times, (Nb, V, Ti) C, mechanical properties

1 Introduction

Critical factors such as frequent natural disasters, which cause substantial economic loss, have aroused people's widespread concern about high-strength rebar. This has necessitated putting forward higher requirements for the performance of high-strength rebars. According to the new national standard GB/T 1499.2-2018 Part 2, the mechanical properties and seismic requirements of hot-rolled ribbed rebars are as follows: yield strength (R_{eL}) ≥ 500 MPa, tensile strength (R_m) ≥ 630 MPa, elongation after fracture (A) ≥ 15%, maximum total elongation (A_{gt}) ≥ 9%, and strain-hardening ratio (R_m^0/R_{eL}^0) ≥ 1.25. The addition of alloying elements in rebar can significantly improve the mechanical properties of high-strength rebar [1–5]. At present, the alloying elements (Nb, V, Ti, etc.) are commonly used to improve the strength of high-strength rebar. The addition of Nb in rebar can promote the improvement of mechanical properties by strain-induced precipitation in austenite [6–9]. The addition of V in rebar can refine the microstructure grains. The addition of Ti in rebar promotes refinement of the microstructure by limiting the grain coarsening in reheating [10]. Many studies have shown that [11–14] composite strengthening of the alloying elements can enhance the fine-grain and precipitation strengthening and reduce production costs.

The influence of the chemical composition of the rebar and the parameters of controlled rolling and controlled cooling on the microstructure and mechanical properties of high-strength rebar has been a research hotspot of researchers [15–17]. Akhtar and Khajuria et al. [18–24] further analyzed and characterized the phase transformation process and the changes in mechanical properties by combining experimental simulations, and the method used in this process can further optimize the heat treatment process. Isothermal time treatment is a critical factor that affects the properties of high-strength rebar. It is also an important control parameter in the process of controlled rolling and controlled cooling.

* **Corresponding author: Zhiying Li,** College of Materials and Metallurgy, Guizhou University, Guiyang, 550025, P. R. China; Guizhou Provincial Key Laboratory of Metallurgical Engineering and Process Energy Saving, Guiyang, 550025, P. R. China, e-mail: lizhiying2015@163.com
Tianyou Wang, Changrong Li, Zeyun Zeng: College of Materials and Metallurgy, Guizhou University, Guiyang, 550025, P. R. China; Guizhou Provincial Key Laboratory of Metallurgical Engineering and Process Energy Saving, Guiyang, 550025, P. R. China
Jie Wang, Fulong Wei: Shougang Shuicheng Iron and Steel Group, Liupanshui, 550033, P. R. China

Isothermal time treatment is the key factor affecting the performance of high-strength rebar. However, it is also an important control parameter in the process of controlled rolling and controlled cooling. By controlling the isothermal time treatment within the optimal range [25], the composite strengthening of Nb, V, Ti, and the precipitation phase can be promoted to play the most significant role so that the experimental rebar obtains the best mechanical properties and meets the national standard. Studies have shown that after the high-strength rebars undergo phase transition due to isothermal treatment, the precipitation enhancement effect of nanoprecipitates on the ferrite matrix is enhanced [26,27]. Huo et al. [28,29] showed that the Ti high-strength rebar is rolled and held at an isothermal temperature of 650°C for 600 s, and the strengthening effect of nanoscale precipitates was the strongest. Joon Chun et al. [30] studied the effect of cooling temperature on the mechanical properties of Nb–V–Ti composite microalloyed rebar. The results showed that the nanoprecipitates distributed on the ferrite matrix had a good precipitation strengthening effect when the experimental rebar was isothermally stored at 650°C for 1 h. Kang et al. [31] also studied the thermoplasticity of microalloyed rebar after holding it at 900 and 1,000°C at different times. The results showed that the samples without special alloying elements (Nb) were not affected by isothermal time, and the samples with Nb and Mn were slightly improved. The thermoplasticity of the two samples with Nb content of 0.031 and 0.062 wt% increased significantly with the increase in isothermal time. Balbi et al. [32] studied duplex steels austenitized at 930°C for 20 min and then annealing at 830°C for 5, 15, 30, 60, and 120 min, and finally water quenching. The results show that isomorph ferrite and martensite are formed at a short annealing time, and polygonal ferrite is formed at a long annealing time. Zheng et al. [33] investigated the effect of different isothermal times at 950°C on the thermoplasticity of the C–Mn rebar. The results showed no significant difference in low isothermal time (less than 500 s), and the thermoplasticity of the rebar was improved after long isothermal time. The findings of the above researchers are summarized in Table 1.

Currently, many researchers have focused on the study of the addition of alloying elements and the controlled rolling and cooling process on the properties of high-strength rebar [34,35]. There are relatively few studies on the effects of different isothermal time treatments at the final cooling temperature on the microstructure transformation, precipitation behavior, and mechanical properties of high-strength rebar. Most studies are carried out on Nb, Nb–Ti, and Nb–V high strength. However, Nb–V–Ti composite microalloying is an important technology to improve the microstructure transformation and mechanical properties of high-strength rebar [36,37]. The combination of composite microalloying and controlled rolling and cooling process is an effective method to improve the strength of the rebar. In this study, the effects of different isothermal time treatments on the microstructure, precipitation behavior, and mechanical properties of high-strength rebars were analyzed at 650°C for 30, 60, 100, and 200 s. By combining the controlled rolling and cooling process with multi-element composite microalloying to obtain the appropriate isothermal time and regulate the optimal alloying element ratios, it provides a theoretical basis and reference for the design of process parameters of high-strength rebars, so that the expected results can be used in the basic application during the development varieties of new rebar.

2 Experimental processes

2.1 Material preparation

In order to control the composition of the experimental rebar, a 500 MPa high-strength seismic rebar was selected as the raw material. Before the thermal simulation, the raw material was a cast billet. The microstructure of the cast billet was coarse ferrite grains and pearlite with large lamellar spacing, as shown in Figure 1. According to the requirements of the new national standard, one added conventional elements (such as C, Si, and Mn) and the other added micro-alloying elements such as Nb, V, and Ti. A set of optimized experimental rebars containing Nb, V, and Ti were designed to be melted in a medium-frequency induction furnace. Then, the ingot (about 15 kg) was forged into a cylindrical rod with a diameter of 40 mm and a height of 60 mm in an Nb-SX2-2.5-12TP box-type resistance furnace on a two-roll hot and cold continuous rolling mill with a diameter of 350 mm and a height of 300 mm. The forging process was as follows: the ingot sample was heated to 1,200°C at a speed of $15°C·s^{-1}$, held for 10 min, and then cooled to 1,000 and 900°C at a speed of $15°C·s^{-1}$. The hot deformation was 40 and 30%, respectively, and the deformation rate was $2\,s^{-1}$, and air-cooled to room temperature.

Carbon equivalent is a requirement in the new national standard GB/T 1499.2-2018, and the new national standard states that the value of carbon equivalent is not greater than 0.55, while the carbon equivalent is also an important criterion for judging the welding performance of rebar. Carbon equivalent C_{eq} (wt%) can be calculated by the following equation [38]:

$$C_{eq} = C + Mn/6 + (Cr + V + Mo)/5 + (Cu + Ni)/15. \quad (1)$$

Table 1: Literature review

Author	Characterization methods	Study results
Fida Hassan and Alwadei [1], Yan et al. [2], Huang et al. [3], Gomez et al. [4], Hassan and Al-Wadei [35], and Yi et al. [36]	Optical microscope (OM)/ BSE/X-ray/SEM	Under the condition of multi-element composite strengthening, the microalloyed steel undergoes hot-rolling and cooling process, the microstructure is more homogenized, and the precipitates are highly diffusely distributed, so that the yield strength and tensile strength can be increased by 5–29.5% and have good strong toughness
Gong et al. [5], Ma et al. [6], Chen et al. [7], Huang et al. [8], Li et al. [9], and Tian et al. [37]	OM/SEM/TEM/EBSD/APT	After the deformation of microalloyed steel, the precipitates formed by the composite strengthening of Nb and Ti/Mo/V are diffusely precipitated and pinned to austenite grain boundaries. In the process of transformation from austenite to ferrite, Nb/Ti/Mo/V composite strengthening precipitates give full effect to fine-grain strengthening and precipitation strengthening, which further refines the ferrite grain size and pearlite lamellar spacing and further improves the strength and plasticity of the steel
Ding et al. [10], Li et al. [11], Zeng et al. [12], and Zhang et al. [13]	SEM/XRD/CLSM/OM/ Nanoindentation/BSE	The addition of alloying elements such as Nb/Ti/V in microalloyed steel plays a different role in strengthening at different heat treatment stages, thus obtaining different proportions of microstructure and precipitate distribution, which further improves the hardness and strength of the steel
Jiang et al. [14], Buken et al. [15], Shen et al. [16], and Furuhara et al. [17]	OM/HRTEM/EBSD/ STEM/XRD	The synergistic strengthening effect between the precipitation behavior of micro-alloying elements and microstructure is determined by designing a rolling model in microalloyed steels in the recrystallization temperature interval and comparing it with experimental results. The evolution of microstructure by micro-alloying elements can be promoted, thus proposing a model for the design of process parameters that correlate precipitate precipitation behavior with tissue evolution
Liu et al. [25], Peng et al. [26], Zhang et al. [27], Huo et al. [28,29], Joon Chun et al. [30], Kang et al. [31], Balbi et al. [32], Zheng et al. [33], and Zhao et al. [34]	SEM/TEM/HRTEM/OM/ XRD/CTEM	By designing a rolling process for microalloyed steel and then setting different isothermal time parameters during cooling phase transformation based on controlled rolling, the precipitation strengthening effect of Nb/V/Ti composite precipitates in the isothermal process is fully utilized. This promotes the diffuse distribution of precipitates and the homogenization of microstructure, which leads to the improvement of tensile and yield strengths

The chemical composition of the experimental rebar was analyzed by a carbon sulfur analyzer, nitrogen hydrogen oxygen analyzer, and inductively coupled plasma analyzer. The chemical composition of the experimental rebar is shown in Table 2.

2.2 Experimental process

The phase change temperature point is an important parameter in the design of the phase change process and the subsequent isothermal cooling process [38]. The test rebar also includes the onset temperature of the phase transformation from ferrite to austenite (Ac_1) and the end temperature of the phase transformation from ferrite to austenite (Ac_3) during heating, and the critical transformation temperatures of the onset transition temperature from austenite to ferrite (Ar_1) and the end temperature of the austenite phase transformation (Ar_3) during cooling. The thermal expansion test was performed on the DIL402C thermal expander, and the forged sample was cut into a

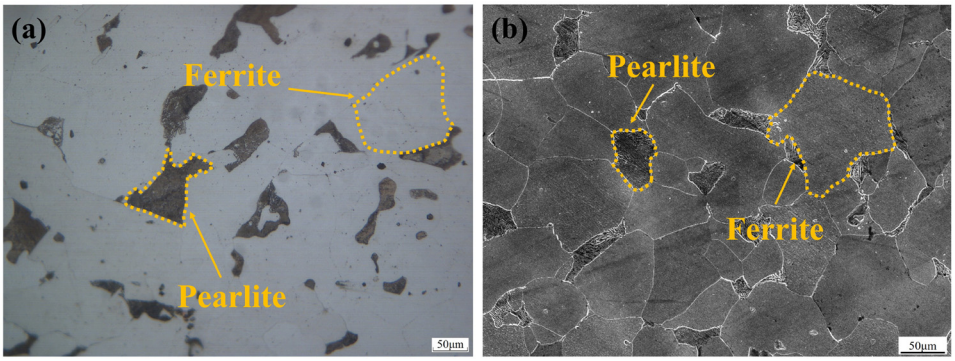

Figure 1: Microstructure of raw materials: (a) OM and (b) SEM.

cylindrical sample of diameter (6 mm) × length (25 mm), heating the sample to 1,250°C at 5°C·s^{-1} and holding it for 5 min, and then cooling it to room temperature at 5°C·s^{-1} to obtain the thermal expansion curve of the test rebar. During the phase transformation from austenite to ferrite, the slope of the thermal expansion curve varies with the volume expansion at different stages. The critical transition temperatures of the test rebars are shown in Table 3.

The critical recrystallization temperature plays an important role in determining microstructural evolution in seismic rebars [34]. Zeng et al. [38] reported the formula for calculating the critical recrystallization temperature (T_{nr}) as follows:

$$T_{nr} = 887 + 464C + (6445Nb - 644\sqrt{Nb}) + (732V - 230\sqrt{V}) + 890Ti + 363Al - 357Si, \quad (2)$$

where T_{nr} refers to the critical recrystallization temperature (°C), and Nb (wt%), V (wt%), Ti (wt%), and C (wt%) refer to the content of Nb, V, Ti, and C in rebar.

According to equation (2), the critical austenite recrystallization temperature (T_{nr}) of the experimental rebar was calculated to be 947°C. In this experiment, the hot-rolling temperatures of the first pass, the second pass, and the third pass were 1,000, 980, and 950°C, respectively, which belong to the rolling within the austenite recrystallization temperature. The hot-rolling temperatures of the fourth and fifth passes were 900 and 850°C, respectively, which were rolled within the austenite non-recrystallization temperature.

According to the results of previous studies and the results of previous studies by the group team [13,26,39–45], the temperature of 650°C was chosen as the final cooling temperature because the optimal microstructure ratio and fine nanoscale diffusely distributed precipitates are obtained after hot rolling at this temperature, and the mechanical properties are substantially enhanced by the joint strengthening effect of both. Therefore, in this study, the temperature of 650°C was chosen as the final cooling temperature and set different isothermal times to investigate the intrinsic relationship between the microstructure precipitation behavior and the mechanical properties of Nb-containing experimental rebars.

Table 3: Critical transformation temperature of the experimental rebars

Ac_1 (°C)	Ac_3 (°C)	Ar_1 (°C)	Ar_3 (°C)
767	795	762	791

The forging samples were processed into rectangular samples (100 mm × 40 mm × 20 mm) by wire cutting. The plane compression experiment was carried out on the Gleeble-3800 thermal simulator. The thermal simulation of the experimental rebar is shown in Figure 2.

All samples were heated to 1,150°C at 20°C·s^{-1} for 10 min to homogenize austenite and dissolve Nb, V, and Ti uniformly. The hot-rolling temperature of five passes was reduced to 1,000, 980, 950, 900, and 850°C at 5°C·s^{-1}, and the deformations of five passes were 0.25, 0.15, 0.1, 0.1, and 0.1, and the compression strain rates of five passes were 2, 0.5, 0.5, 0.5, and 0.5 s^{-1}. After hot

Table 2: Chemical composition of the experimental rebar (mass fraction, %)

C	O	S	P	Si	Nb	V	Ti	Mn	C_{eq}
0.17	0.0082	0.012	0.018	0.229	0.013	0.055	0.015	1.552	0.44

rolling, the samples were rapidly cooled to 650°C, holding for 30, 60, 100, and 200 s. Finally, the samples were cooled to 200°C with 0.5°C·s^{-1} and then air-cooled.

2.3 Test method

The rectangular samples with the dimension of 10 mm × 10 mm × 10 mm were processed by thermal simulation. After coarse and fine grinding, the samples were polished by a PG-IA metallographic specimen polishing machine. The microstructure and the existence of the second phase were observed by SUPRA40 field emission scanning electron microscope. The Ipwin32 software image analyzer was utilized to count the proportion of ferrite and pearlite, and the ferrite grain size and pearlite lamellar spacing were measured by the Nano Measurer software image analyzer.

The central part of the thermal simulation specimen was used as the tensile specimen. According to the national standard, the tensile specimen with the dimension of 120 mm × 15 mm × 2 mm was processed using the GB/T 228.1-2010 tensile test method at room temperature. The tensile test machine (MTS810) was used at room temperature to stretch at a 10^{-2} s^{-1} strain rate.

In order to observe the precipitation behavior of Nb/Ti/V, the sample was further processed into a small round plate with a diameter (5 mm) × thickness (2 mm). The sample was grinded to 0.1 mm thickness and mechanically thinned to 30 μm. Then, the ion thinning was carried out to prepare the transmission electron microscope sample. The precipitation behavior of Nb/Ti/V was analyzed by TECNAI G2F30 S-TWIN high-resolution electron microscope at 200 kV. The composition of Nb/Ti/V precipitates was analyzed by electron spectrometer and transmission electron microscope. Selected area electron diffraction (SAED) spectra of diffraction ring Fourier transform were obtained by Digital Micrograph software.

3 Results

3.1 Effect of isothermal time on the microstructure

The scanning electron microscopy (SEM) morphology of the experimental rebar under four different isothermal time treatments is shown in Figure 3. The proportion statistics of pearlite and ferrite under four different isothermal time treatments are shown in Figure 4.

Figures 3 and 4 show that the microstructure of the experimental rebar is mainly composed of ferrite and pearlite. The ferrite is mostly polygonal, and the pearlite is mostly lamellar, uniformly distributed on the ferrite matrix. Figure 4 shows that with the increase in isothermal time, the proportion of ferrite increases from 54.92 to 68.12%, and the proportion of pearlite increases from 15.88 to 30.08%. After grain refinement, the ferrite area decreases, and the grain boundary increases. This provides favorable conditions for the nucleation of pearlite and increases the proportion of pearlite microstructure. In the rolling process, the carbides formed by strain

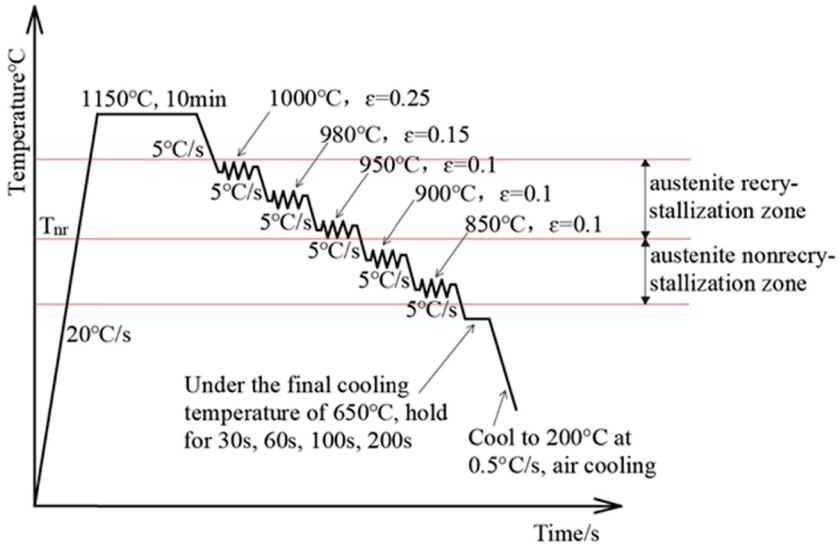

Figure 2: Thermal simulation process of the experimental rebar.

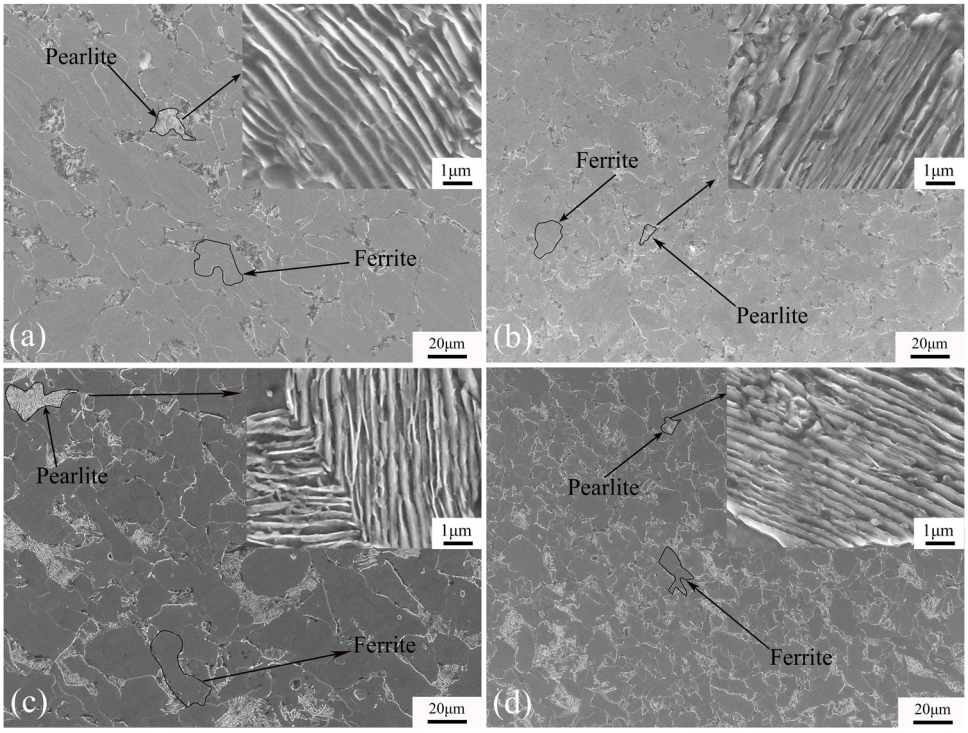

Figure 3: SEM morphology under the conditions of different isothermal times: (a) 30 s, (b) 60 s, (c) 100 s, and (d) 200 s.

induction precipitate around the austenite [46]. The carbides consume large amounts of carbon, reducing the stability of supercooled austenites and favoring the formation of pearlites and ferrites during phase transitions. The nucleation of pearlite requires sufficient time to make ferrite and cementite grow together, which mainly depends on the diffusion of carbon atoms. Therefore, sufficient isothermal time is crucial for the diffusion of carbon atoms [45]. Shanmugam et al. [47] also mentioned the formation of layered pearlite in V- and Nb-microalloyed rebars. They also explained that the equilibrium growth of pearlite needs enough time, and the short isothermal time will lead to insufficient carbon diffusion, which affects the nucleation rate of pearlite. Rothleutner et al. [48] mentioned that micro-alloying elements are usually used to modify ferrite and pearlite in rebar to improve strength, fatigue resistance, and wear resistance. In this study, with the increase in isothermal time, the ferrite and pearlite distribution ratio was improved, thereby improving the mechanical properties of the rebar.

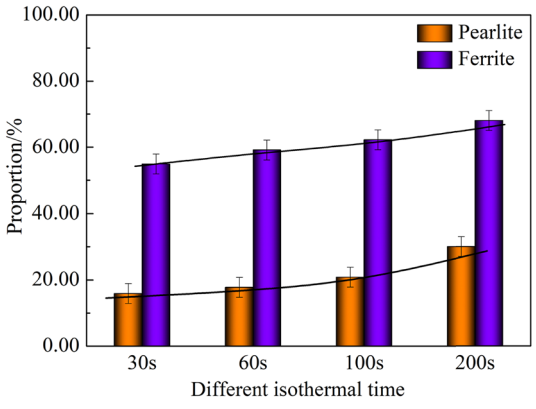

Figure 4: Proportion statistics of pearlite and ferrite under the conditions of different isothermal times.

3.2 Effect of isothermal time on the grain size

A total of 100 metallographic images and 100 pearlite lamellar SEM images of the experimental rebar were selected under four different isothermal time treatments. Ten curves were intercepted in each image by using Nano Measurer image analysis software. The data of 100 images were counted, and the average value was taken. The size of ferrite and the pearlite lamellar spacing were counted, as shown in Figure 5.

Figure 5 shows that the ferrite grain sizes of the experimental rebar are 10.632, 10.513, 10.224, and 8.326 μm, and the pearlite lamellar spacing is 0.230, 0.213, 0.178, and 0.142 μm, respectively, after holding for 30, 60, 100, and 200 s at 650°C

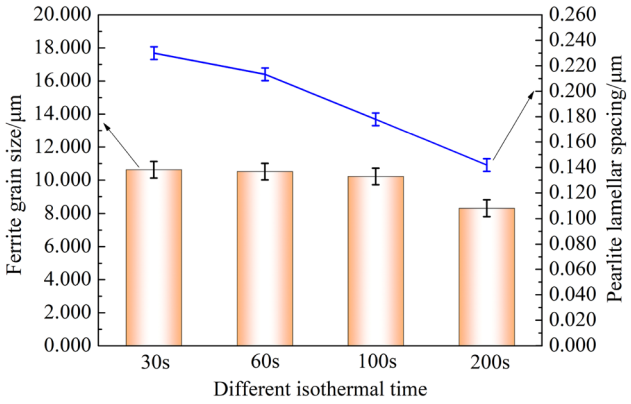

Figure 5: Ferrite grain size and pearlite lamellar spacing of the experimental rebar under the conditions of different isothermal times.

and then air-cooled. When the isothermal time reached 200 s, the grain distribution was more uniform, the ferrite grain size was reduced to 8.326 μm, and the pearlite lamellar spacing was refined to 0.142 μm.

Many studies [8,49] have shown that the reduction of ferrite grain size can increase the grain boundary area, thereby reducing stress concentration, increasing the uniform distribution ability of transient deformation, and improving the yield strength of the rebar. Other studies [50,51] have pointed out that the increase in yield strength is related to the ultrafine grain size of the microstructure. In this study, the ferrite grain size decreases, the pearlite lamellar becomes finer, and the yield strength increases.

3.3 Effect of isothermal time on the precipitation behavior

The (Nb, V, and Ti) C precipitates of the experimental rebar after treatment for 60 s are shown in Figure 6. The (Nb, V, and Ti) C precipitates in the experimental rebar treated for 200 s are shown in Figure 7(a)–(d).

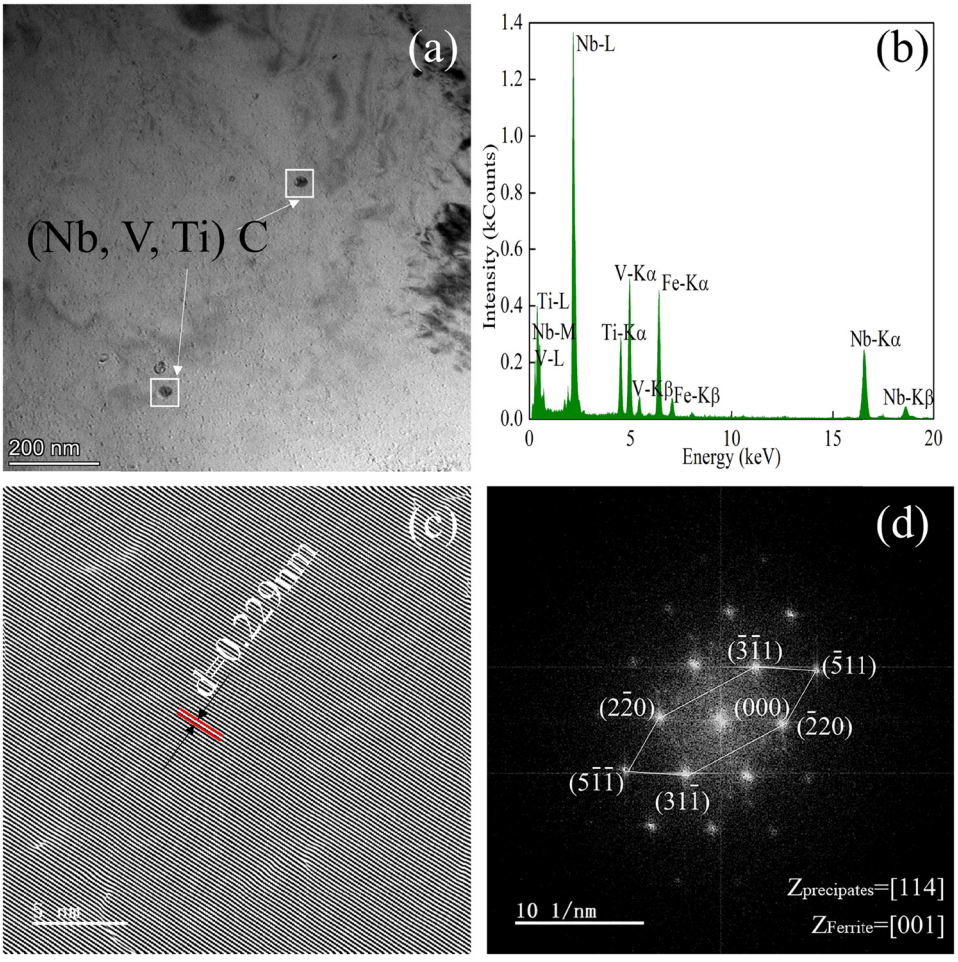

Figure 6: TEM images of (Nb, V, and Ti) C precipitates in the experimental rebar at 60 s. (a) Morphology, (b) energy-dispersive spectrometry (EDS), (c) lattice fringes, and (d) SAED.

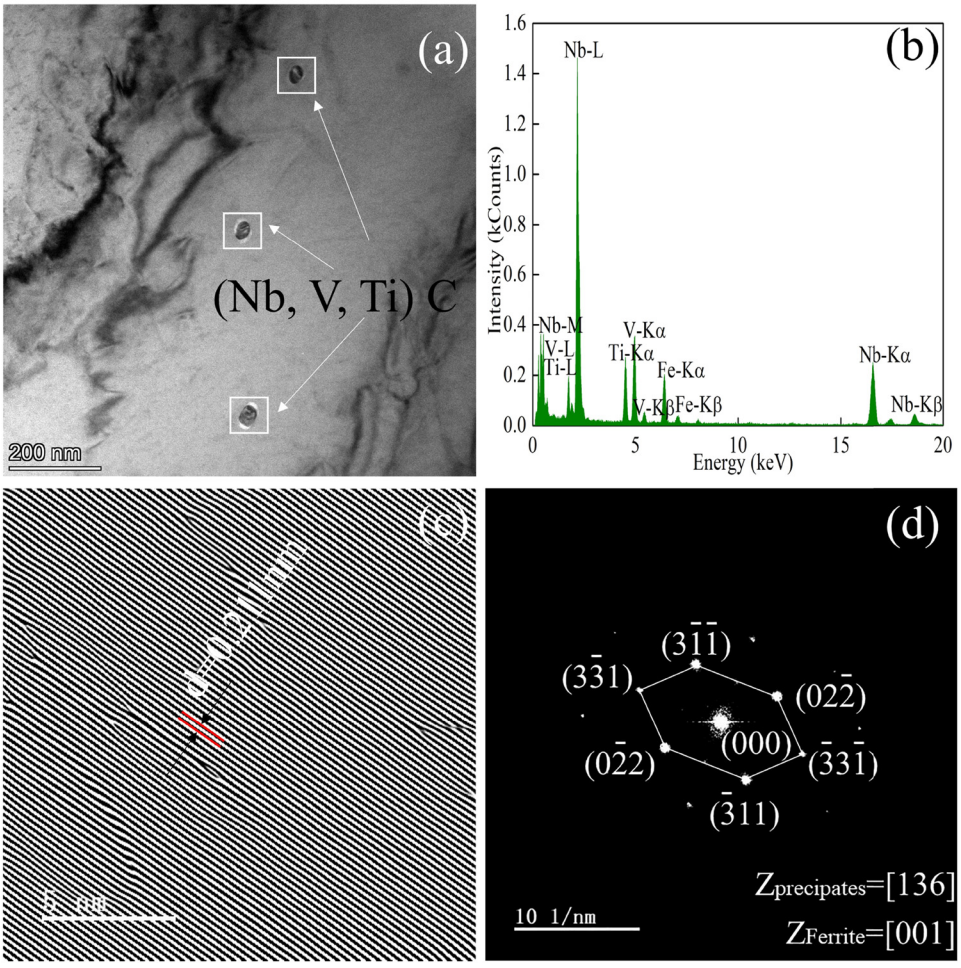

Figure 7: TEM images of (Nb, V, and Ti) C precipitates in the experimental rebar at 200 s. (a) Morphology, (b) EDS, (c) lattice fringes, and (d) SAED.

Figure 8 shows the average particle size statistics of the precipitates under different isothermal time treatments.

The shape of (Nb, V, and Ti) C precipitates in the experimental rebar is mainly round. The size of precipitates is 25–35 nm, as shown in Figures 6(a) and 7(a). Figure 8 shows the average particle size changes of (Nb, V, and Ti) C precipitates at isothermal times of 30, 60, 100, and 200 s are 34.014, 32.155, 30.047, and 29.916 nm, respectively. Therefore, with the increase in isothermal time, the size of precipitates decreased from 34.014 to 29.916 nm. Figures 6(b) and 7(b) show the EDS spectra of the two precipitates. The diffraction peaks of the precipitates are mainly Nb, followed by V and Ti, and the mass fraction ratios are 1.5:0.4:0.3 and 1.4:0.5:0.4, respectively. Figures 6(c) and 7(c) are the diffraction lattice fringe patterns obtained by the inverse Fourier transform of high-resolution images. It is observed that the crystal plane spacing of the precipitates is 0.229 nm at 60 s and 0.211 nm at 100 s. The SAED in Figures 6(d) and 7(d) shows that there is a certain orientation relationship between (Nb, V, Ti) C precipitates and ferrite [52]: (5(—)11) (Nb, V, Ti) C‖(100)α and [114] (Nb, V, Ti) C‖[001]α and (022(—))(Nb, V, Ti) C‖(100)α and [136](Nb, V, Ti) C‖[001]α.

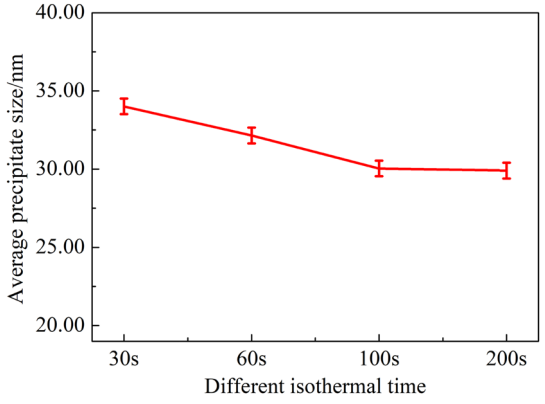

Figure 8: Statistics of average particle size of precipitates under the conditions of different isothermal times.

High-density dislocation wall can also be observed in Figures 6(a) and 7(a). The dislocation is closely related to the strain hardening of the rebar. The recrystallization process is controlled by alloying and intragranular nanoprecipitation, which is easy to form an ultrafine grain structure. The nanoprecipitation improves the thermal stability of ultrafine grain structures by the effect of pinning. When holding for 600 s, the hardness value of the sample increased due to the contribution of the (Nb and Ti) (C and N) phase precipitation to the hardness. The grain size of precipitates decreased under different isothermal times. The number of precipitates increased and dispersed in the grain boundary and interior, significantly increasing the strengthening effect [53–55].

Combined with the relationship between isothermal time and mechanical properties in Figure 9, the strength of the rebar increases with the increase in isothermal time, which is consistent with the general rule of the effect of precipitation strengthening on mechanical properties. A sufficient isothermal time allows the C atoms to precipitate continuously from the austenite and diffuse sufficiently into the matrix, while the strength is enhanced due to the increased number and more diffuse distribution of alloy carbides, which also enhance the interaction with dislocations. With the increase in isothermal time, the presence of precipitates can also be observed between the ferrite and pearlite phases, and these spherical forms of precipitates reduce the stress concentration effect and can also play a precipitation strengthening role, reducing the strength loss due to ferrite generation [3,8,45]. As can be seen in Figures 6 and 7, in addition to the presence of precipitates, dislocation aggregation can also be seen. With the interaction between the two, the precipitates can pin on the dislocations, making it possible to maintain high strength at high temperatures. With the increase in isothermal time, dislocation density decreases at some of the weaker locations of grain boundaries. When the precipitation phase pins the grain boundaries, the dislocation density at the grain boundaries increases and stabilizes, resulting in dislocation strengthening and increasing the strength of the rebar [7,34,37,38,41].

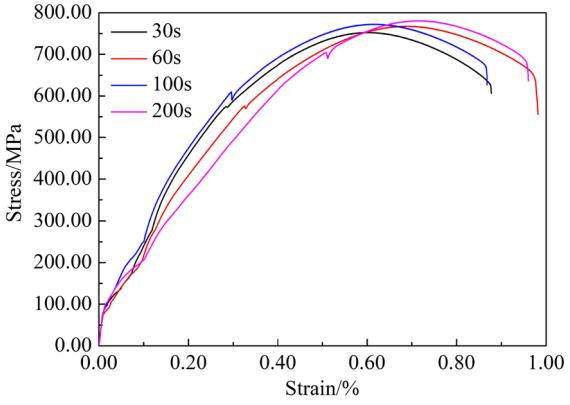

Figure 9: Stress–strain curves of the experimental rebar under the conditions of different isothermal times.

3.4 Effect of isothermal time on the mechanical properties

In order to characterize the stress–strain curve of the experimental rebar under different isothermal time treatments, the experimental rebar was stretched. The stress–strain diagram is shown in Figure 9, and the stress–strain data are shown in Table 4.

With the increase in isothermal time, the tensile strength and yield strength of the experimental rebar gradually increase, and the strength–yield ratio gradually decreases. The stress–strain curve of the experimental rebar has a yield platform under different isothermal time conditions, as shown in Figure 9. When the isothermal time was 200 s, the tensile strength and yield strength of the experimental rebar were the highest at 780.713 and 621.434 MPa, respectively. Zeng [45] pointed out in the study on the effect of final cooling temperature on the properties of rebar that the precipitated phase of carbides was easy to precipitate on the ferrite matrix and dislocation line, which refined the lamellar spacing of ferrite grains and pearlite and improved the mechanical properties of rebar. Wang et al. [56] predicted the mechanical properties of rebar containing ferrite and pearlite. They pointed out that the tensile strength increased with the increase in pearlite volume fraction, which was consistent with the results of this study. Bu et al. [57,58] showed a remarkable strengthening effect when nanocarbides precipitate in the ferrite phase.

It is obvious from Figure 8 that the mechanical properties of the experimental rebar improved with the increase

Table 4: Tensile data of the experimental rebar under different isothermal time conditions

Rebar	Tensile strength (MPa)	Yield strength (MPa)	Strength yield ratio	Elongation after breaking (%)
30 s	752.477	574.714	1.314	32.752
60 s	767.592	575.764	1.337	36.253
100 s	772.381	604.585	1.285	42.504
200 s	780.713	621.434	1.261	43.131

in isothermal time. Because of the synergy between the composite strengthening of micro-alloying elements such as Nb, V, and Ti and isothermal time, the improvement of mechanical properties of the experimental steel is mainly due to two aspects: (1) With the addition of micro-alloying elements in rebar, the micro-alloying elements can solidly be soluble in rebar and produce aggregation at grain boundaries, which can play a role in inhibiting grain boundary growth and migration, reducing the driving force of grain growth and obtaining the purpose of grain refinement effectively, thereby improving the strength. During the transformation of pearlite, the diffusion rate of micro-alloying elements is less than that of carbon atoms, and the carbon atoms solidly dissolved in the rebar reduce the nucleation and growth rate of cementite, extend the gestation period of pearlite transformation, increase the supercooling degree, and refine the ferrite grain size and pearlite lamellar spacing [59–63]. The refinement of the pearlite lamellar structure can effectively hinder the sprouting and expansion of cracks and improve the tensile properties of the experimental rebar. From the above results, it can be seen that with the increase in isothermal time, the ferrite size and pearlite lamellar spacing are further refined and dislocations are aggregated in ferrite and pearlite. When the ferrite size and pearlite lamellar are reduced, it makes it difficult for dislocations to move, which makes the tensile strength increase; (2) during the heat treatment of the experimental rebar, a large number of composite precipitates are precipitated at grain boundaries or dislocations due to strain-induced effects. These precipitates pin on grain boundaries to further refine the austenite grains, which are accompanied by a large number of composite precipitates diffusely precipitated on ferrite during the transformation of austenite to ferrite. With the increase in isothermal time, the precipitates easily occur in the dispersive distribution, and the precipitates interact with dislocations, causing obstruction to dislocation movement and significantly improving the strength of the experimental rebar. During the tensile process, when dislocations have difficulty bypassing these non-deformable nanoscale precipitated phases, the dislocations will be subjected to greater resistance and thus require greater applied stress to allow the dislocations to continue to slip past the precipitated phases, thus leading to an increase in the strength of the experimental rebar [64–68]. The resistance to dislocation movement is increased by the precipitates, and the higher the resistance, the higher the yield strength.

3.5 Strengthening mechanism analysis

The results in Figure 9 and Table 4 show that the mechanical properties of the experimental rebar are significantly affected by the length of the isothermal time, and the microstructure of the material is also closely related to its strength. The contribution of different strengthening mechanisms to the yield strength of rebar can be expressed by the following equation [69,70]:

$$\sigma_y = \sigma_0 + \sigma_{ss} + \sigma_{GB} + \sigma_{pre} + \sigma_t, \tag{3}$$

where σ_y is the total yield strength; σ_0 is the friction coefficient of an iron crystal, usually 54 MPa; σ_{ss} is the solid solution strengthening; σ_{GB} is the fine-grain strengthening; σ_{pre} is the precipitation strengthening; and σ_t is the phase transformation strengthening.

For high-strength seismic rebars, the microstructure of the experimental rebar is composed of ferrite and pearlite. Important micro-alloying elements such as Mn, Si, and P can form a solid solution in the rebar. The results of many researchers show that [71] the solid solution strengthening amount of microalloyed rebar can be quantitatively expressed as the following equation:

$$\sigma_{ss} = 37[\mathrm{Mn}] + 83[\mathrm{Si}] + 680[\mathrm{P}], \tag{4}$$

where [Mn], [Si], and [P] refer to the mass fraction of the experimental rebar, %.

According to equation (4), the solid solution strengthening increment of Mn, Si, and P on the experimental rebar is 123.29 MPa.

Grain refinement is one of the important means of improving the strength and plasticity of rebar [72]. Due to the addition of micro-alloying elements in the rebar, the second phase precipitates in the strain-induced process refine the grain, and the strengthening effect is further enhanced [14]. Grain refinement follows the Hall–Petch equation [73]:

$$\sigma_{GB} = kd^{-\frac{1}{2}}, \tag{5}$$

where k is the grain strengthening coefficient, and its value is related to the grain boundary structure. Usually, the value is 15–18 MP·mm$^{-0.5}$, where the value is 15.1 MP·mm$^{-0.5}$, d is the average diameter of ferrite grains, and the unit is mm.

Figure 5 and equation (5) show that the ferrite grain size decreases gradually with the increase in isothermal time, so the contribution rate to yield strength increases gradually. The calculation shows that under different isothermal time conditions of 30, 60, 100, and 200 s, the contribution of grain refinement to yield strength is 146.46, 147.29, 149.37, and 165.54 MPa, respectively.

The precipitation strengthening of the experimental rebar mainly comes from the precipitation of carbides, which results from the interaction between precipitates and dislocations. The strain-induced precipitation of (Nb, V, Ti) C in austenite can play a role in precipitation strengthening. Precipitation strengthening is related to the volume and size of precipitates in rebar, which can be calculated by the Ashby–Orowan equation [74]:

$$\sigma_{\text{pre}} = 5.9f^{-0.5} \ln\left(\frac{x}{2.5 \times 10^{-4}}\right), \quad (6)$$

where σ_{pre} is the precipitation strengthening increment (MPa), x is the average particle diameter (nm), f is the precipitation volume fraction (%), and the precipitation volume fraction of NbC, TiC, and VC is calculated using the following equation [75]:

$$f_v = (\Sigma \text{M}_\text{i} - \Sigma[\text{M}_\text{i}] + \text{C} - [\text{C}])\frac{\rho_{\text{Fe}}}{\rho_{\text{MC}}}, \quad (7)$$

where [Mi] (Mi = Nb, V, Ti) is the solid solution of microalloying element Mi in ferrite; Mi is the content of microalloying element Mi in rebar, wt% (Table 2); [C] is the solid solution amount of C in ferrite; C is the content of C in rebar, wt% (Table 2); ρ_{Fe} and ρ_{MC} are the density of Fe and MC (MC = NbC, TiC, and VC), namely, $\rho_{\text{Fe}} = 7.8\ \text{g/cm}^2$, $\rho_{\text{NbC}} = 8.47\ \text{g/cm}^2$, $\rho_{\text{TiC}} = 4.93\ \text{g/cm}^2$, and $\rho_{\text{VC}} = 5.77\ \text{g/cm}^2$.

Using the solid solubility product formula of MC (MC = NbC, TiC, and VC) and stoichiometric ratio, the solid solubility of related elements (Nb, Ti, V, and C) in ferrite can be calculated. The solid solubility product formula of MC (MC = NbC, TiC, and VC) in ferrite can be expressed as [76]:

$$\lg\{[\text{Nb}]\cdot[\text{C}]\}_\alpha = 5.43 - \frac{10960}{T}, \quad (8)$$

$$\lg\{[\text{Ti}]\cdot[\text{C}]\}_\alpha = 4.4 - \frac{9575}{T}, \quad (9)$$

$$\lg\{[\text{V}]\cdot[\text{C}]\}_\alpha = 4.55 - \frac{8300}{T}, \quad (10)$$

where [Mi] (Mi = Ti, Nb, V) is the solid solution of Mi element in ferrite, [C] is the solid solution of carbon in ferrite, α is the solid solution product of ferrite, and T is the solid solution temperature. It is concluded that the contribution of precipitation strengthening to yield strength is 171.09, 205.34, 219.88, and 299.45 MPa, respectively, under the different isothermal times of 30, 60, 100, and 200 s.

Pearlite is a strengthening phase, which can improve the strength of rebars. According to equation (3) combined with Figure 5, the increment in pearlite phase transformation strengthening was studied. The experimental rebar has a certain number of pearlite phase transformations (Figure 3). With the increase in isothermal time, the increment in phase transformation strengthening increases from 84.99 to 93.59 MPa. This indicates that the effect of phase transformation strengthening is enhanced.

The comparison of the contribution of each strengthening mechanism to yield strength is shown in Figure 10(a), and the comparison between the theoretical value and the experimental value is shown in Figure 10(b).

The comparison of various strengthening mechanisms follows the following trend: the precipitation strengthening increment > the fine-grain strengthening increment > the solid solution strengthening increment > the phase transformation strengthening increment. The contribution of fine-grain strengthening and precipitation strengthening to yield strength is the highest. In the production, composite strengthening, controlled rolling, and controlled cooling are combined to make fine-grain strengthening. Precipitation strengthening plays the most significant role so that the properties of rebar are further improved.

With the increase in isothermal time, the yield strength of the experimental rebar is gradually increased. The theoretical calculation value is gradually increased, and the difference between the experimental and theoretical values is not significant, indicating that the analysis of the strengthening mechanism is correct.

4 Conclusions

The microstructural transformation, the precipitation behavior, and the mechanical properties of the high-strength rebar under different isothermal time conditions were studied through various characterization methods and thermal simulation machines. The relationship between microstructure transformation, precipitation behavior, and mechanical properties was summarized, and the following conclusions were obtained:

(1) With the increase in isothermal time from 30 to 200 s, the microstructure of the experimental rebar is mainly composed of ferrite and pearlite. The ferrite grain size decreases from 10.632 to 8.326 μm, the pearlite lamellar spacing decreases from 0.230 to 0.142 μm, and the ferrite proportion increases from 54.92 to 68.12%. The pearlite proportion increases from 15.88 to 30.08%.
(2) With the increase in isothermal time from 30 to 200 s, the nanoscale precipitates continued to precipitate

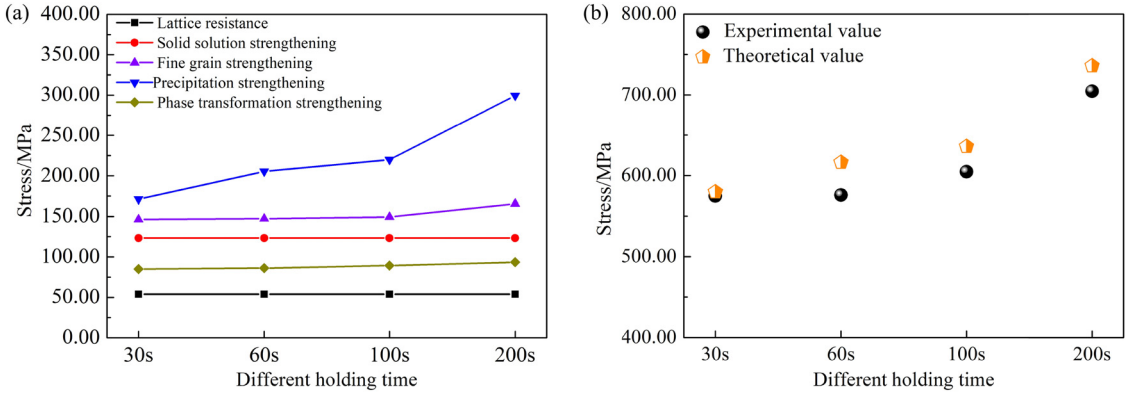

Figure 10: Comparison of strengthening mechanism: (a) contribution of strengthening mechanism and (b) comparison of theoretical strength and actual strength.

elliptically on the ferrite matrix and grain boundary. The size decreased from 34.014 to 29.916 nm, which was more evenly distributed on the ferrite matrix and grain boundary.

(3) With the increase in isothermal time from 30 to 200 s, the yield strength of the experimental rebar increases from 574.714 to 621.434 MPa, and the tensile strength increases from 752.477 to 780.713 MPa. The strengthening effect of precipitation strengthening and fine-grain strengthening is gradually enhanced, which is an effective strengthening method to improve the strength of high-strength rebar.

Acknowledgements: The authors gratefully acknowledge financial support from the institution of the National Natural Science Foundation of China (Grant Number: 52074095) and the Guizhou Provincial Science and Technology Projects ([2022] General 053).

Funding information: This work was supported by Guizhou Provincial Science and Technology Projects ([2022] 053) and supported by National Natural Science Foundation of China (Grant Number: 52074095).

Author contributions: Tianyou Wang: writing – original draft, writing – review and editing, formal analysis, methodology, project administration; Zhiying Li: writing – review and editing, methodology, formal analysis; Jie Wang: visualization; Changrong Li: data curation; Zeyun Zeng: resources; Fulong Wei: investigation.

Conflict of interest: The authors declare no conflict of interest.

Data availability statement: All authors can confirm that all data used in this article can be published in the Journal "High Temperature Materials and Processes."

References

[1] Fida Hassan, S., and H. Alwadei. Ultrahigh strength ductile microalloyed steel with a very low yield ratio developed by quenching and partitioning heat treatment. *Scientific Reports*, Vol. 12, No. 1, 2022, pp. 1–11.

[2] Yan, S., X. Liu, T. Liang, J. Chen, and Y. Zhao. Effect of micro-alloying elements on microstructure and mechanical properties in C-Mn-Si quenching and partitioning (Q&P) steels. *Steel Research International*, Vol. 90, No. 1, 2019, id. 1800257.

[3] Huang, S., C. Li, Z. Li, C. Zhuang, Z. Zeng, and J. Wang. Effect of thermal simulation process on microstructure of seismic steel bars. *Materials*, Vol. 15, No. 10, 2022, id. 3438.

[4] Gomez, M., P. Valles, and S. F. Medina. Evolution of microstructure and precipitation state during thermomechanical processing of a X80 microalloyed steel. *Materials Science and Engineering: A*, Vol. 528, No. 13–14, 2011, pp. 4761–4773.

[5] Gong, P., E. J. Palmiere, and W. M. Rainforth. Thermomechanical processing route to achieve ultrafine grains in low carbon microalloyed steels. *Acta Materialia*, Vol. 119, 2016, pp. 43–54.

[6] Ma, X., C. Miao, B. Langelier, and S. Subramanian. Suppression of strain-induced precipitation of NbC by epitaxial growth of NbC on pre-existing TiN in Nb-Ti microalloyed steel. *Materials & Design*, Vol. 132, 2017, pp. 244–249.

[7] Chen, L., C. Li, and J. Wei. Effect of thermal deformation and Nb element action on the organization and performance of steel. *Materials Research Express*, Vol. 9, No. 5, 2022, id. 056518.

[8] Huang, S., C. Li, Z. Li, Z. Zeng, Y. Zhai, J. Wang, et al. Quantitative analysis of microstructure and mechanical properties of Nb-V microalloyed high-strength seismic reinforcement with different Nb additions. *High Temperature Materials and Processes*, Vol. 40, No. 1, 2021, pp. 300–309.

[9] Li, N., W. Kingkam, R. Han, M. Tang, Y. Yao, H. Zhang, et al. Effect of deformation parameters on microstructural evolution during hot compression of Nb–V–Mo microalloyed steel. *Materials Research Express*, Vol. 7, No. 6, 2020, id. 066521.
[10] Ding, W., Z. Fan, and Y. Yang. Effect of Ti addition on the wear resistance of low alloy steel. *Transactions of the Indian Institute of Metals*, Vol. 75, No. 11, 2022, pp. 2857–2866.
[11] Li, G., Z. Hong, and Q. Yan. The influence of microstructure on the rolling contact fatigue of steel for high-speed-train wheel. *Wear*, Vol. 342-343, 2015, pp. 349–355.
[12] Zeng, D., L. Lu, N. Zhang, Y. Gong, and J. Zhang. Effect of different strengthening methods on rolling/sliding wear of ferrite–pearlite steel. *Wear*, Vol. 358–359, 2016, pp. 62–71.
[13] Zhang, Y. J., G. Miyamoto, K. Shinbo, T. Furuhara, T. Ohmura, T. Suzuki, et al. Effects of transformation temperature on VC interphase precipitation and resultant hardness in low-carbon steels. *Acta Materialia*, Vol. 84, 2015, pp. 375–384.
[14] Jiang, S., H. Wang, Y. Wu, X. Liu, H. Chen, M. Yao, et al. Ultrastrong steel via minimal lattice misfit and high-density nanoprecipitation. *Nature*, Vol. 544, No. 7651, 2017, pp. 460–464.
[15] Buken, H., P. Sherstnev, and E. Kozeschnik. Simultaneous precipitation and recrystallization during hot deformation of Ti, Nb and V microalloyed steel. *Materials Science Forum*, Vol. 879, 2016, pp. 2463–2467.
[16] Shen, W., C. Zhang, L. Zhang, Q. Xu, Y. Xu, and L. Bie. Investigation of recrystallization behavior of large sized Nb–V microalloyed steel rod during thermomechanical controlled processing. *Journal of Materials Research*, Vol. 32, No. 12, 2017, pp. 2389–2396.
[17] Furuhara, T., T. Chiba, T. Kaneshita, H. Wu, and G. Miyamoto. Crystallography and interphase boundary of martensite and bainite in steels. *Metallurgical and Materials Transactions A*, Vol. 48, No. 6, 2017, pp. 2739–2752.
[18] Akhtar, M., A. Khajuria, J. K. Sahu, J. Swaminathan, R. Kumar, R. Bedi, et al. Phase transformations and numerical modelling in simulated HAZ of nanostructured P91B steel for high temperature applications. *Applied Nanoscience*, Vol. 8, No. 7, 2018, pp. 1669–1685.
[19] Akhtar, M., and A. Khajuria. The synergistic effects among crystal orientations, creep parameters, local strain, macro–microdeformation, and polycrystals' hardness of boron alloyed P91 steels. *Steel Research International*, Vol. 93, No. 9, 2022, id. 2100819.
[20] Akhtar, M., and A. Khajuria. Effects of prior austenite grain size on impression creep and microstructure in simulated heat affected zones of boron modified P91 steels. *Materials Chemistry and Physics*, Vol. 249, 2020, id. 122847.
[21] Akhtar, M., and A. Khajuria. Probing true creep-hardening interaction in weld simulated heat affected zone of P91 steels. *Journal of Manufacturing Processes*, Vol. 46, 2019, pp. 345–356.
[22] Akhtar, M., A. Khajuria, M. K. Pandey, I. Ahmed, and R. Bedi. Effects of boron modifications on phase nucleation and dissolution temperatures and mechanical properties in 9%Cr steels: alloy design. *Materials Research Express*, Vol. 6, No. 12, 2019, id. 1265k3.
[23] Akhtar, M., A. Khajuria, V. S. Kumar, R. K. Gupta, and S. K. Albert. Evolution of microstructure during welding simulation of boron modified P91 steel. *Physics of Metals and Metallography*, Vol. 120, No. 7, 2019, pp. 672–685.
[24] Khajuria, A., M. Akhtar, R. Bedi, R. Kumar, M. Ghosh, C. R. Das, et al. Microstructural investigations on simulated intercritical heat-affected zone of boron modified P91-steel. *Materials Science and Technology*, Vol. 36, No. 13, 2020, pp. 1407–1418.
[25] Liu, K., T. Q. He, X. L. Wan, K. Bhandari, and K. M. Wu. The effect of isothermal holding on the microstructures and mechanical properties of a low carbon alloy steel. *Materials Characterization*, Vol. 62, No. 3, 2011, pp. 340–345.
[26] Peng, Z., L. Li, S. Chen, X. Huo, and J. Gao. Isothermal precipitation kinetics of carbides in undercooled austenite and ferrite of a titanium microalloyed steel. *Materials & Design*, Vol. 108, 2016, pp. 289–297.
[27] Zhang, K., Z. Li, F. Sui, Z. Zhu, X. Zhang, and X. Sun. Effect of cooling rate on microstructure evolution and mechanical properties of Ti-V-Mo complex microalloyed steel. *Acta Metallurgica Sinica*, Vol. 5401, 2017, pp. 31–38.
[28] Huo, X., K. He, J. Xia, L. Li, and S. Chen. Isothermal transformation and precipitation behaviors of titanium microalloyed steels. *Journal of Iron and Steel Research International*, Vol. 28, No. 3, 2021, pp. 335–345.
[29] Huo, X. D., L. J. Li, Z. W. Peng, and S. J. Chen. Effects of TMCP schedule on precipitation, microstructure and properties of Ti-microalloyed high strength steel. *Journal of Iron and Steel Research International*, Vol. 23, No. 6, 2016, pp. 593–601.
[30] Joon Chun, E., H. Do, S. Kim, D. Nam, Y. Park, and N. Kang. Effect of nanocarbides and interphase hardness deviation on stretch-flangeability in 998 MPa hot-rolled steels. *Materials Chemistry and Physics*, Vol. 140, No. 1, 2013, pp. 307–315.
[31] Kang, M. H., J. S. Lee, Y. M. Koo, S. J. Kim, and N. H. Heo. The Mechanism of Hot Ductility Loss and Recovery in Nb-Bearing Low Alloy Steels. *Metallurgical and Materials Transactions A*, Vol. 45, No. 10, 2014, pp. 4302–4306.
[32] Balbi, M., I. Alvarez-Armas, and A. Armas. Effect of holding time at an intercritical temperature on the microstructure and tensile properties of a ferrite-martensite dual phase steel. *Materials Science and Engineering: A*, Vol. 733, 2018, pp. 1–8.
[33] Zheng, Z., H. Yu, Z. Liu, T. Xu, and R. D. K. Misra. Mechanism of hot ductility loss in C–Mn steels based on nonequilibrium grain boundary segregation of impurities. *Journal of Materials Research*, Vol. 30, No. 10, 2015, pp. 1701–1714.
[34] Zhao, L., L. Qian, Q. Zhou, D. Li, T. Wang, Z. Jia, et al. The combining effects of ausforming and below-Ms or above-Ms austempering on the transformation kinetics, microstructure and mechanical properties of low-carbon bainitic steel. *Materials & Design*, Vol. 183, 2019, id. 108123.
[35] Hassan, S. F., and H. Al-Wadei. Heterogeneous microstructure of low-carbon microalloyed steel and mechanical properties. *Journal of Materials Engineering and Performance*, Vol. 29, No. 11, 2020, pp. 7045–7051.
[36] Yi, X., L. Sheng, G. Fu, K. Sun, Q. Yang, H. Wang, et al. Insights into the martensitic transformation kinetics and mechanical properties of quaternary Ti–Ni–Nb–V shape memory alloys. *Journal of Materials Research and Technology*, Vol. 19, 2022, pp. 557–565.
[37] Tian, Y., H. Yu, T. Zhou, K. Wang, and Z. Zhu. Revealing morphology rules of MX precipitates in Ti-V-Nb multi-microalloyed steels. *Materials Characterization*, Vol. 188, 2022, id. 111919.

[38] Zeng, Z., C. Li, Z. Li, Y. Zhai, J. Wang, and Z. Li. Effect of Nb content and thermal deformation on the microstructure and mechanical properties of high-strength anti-seismic rebar. *Materials Science and Engineering: A*, Vol. 840, 2022, id. 142929.
[39] García-Sesma, L., B. López, and B. Pereda. Effect of coiling conditions on the strengthening mechanisms of Nb microalloyed steels with high Ti addition levels. *Materials Science and Engineering: A*, Vol. 748, 2019, pp. 386–395.
[40] Natarajan, V. V., S. Liu, V. S. A. Challa, R. D. K. Misra, D. M. Sidorenko, M. D. Mulholland, et al. Processing-structure-mechanical property relationship in Ti-Nb microalloyed steel: Continuous cooling versus interrupted cooling. *Materials Science and Engineering: A*, Vol. 671, 2016, pp. 254–263.
[41] Sanz, L., B. Pereda, and B. López. Effect of thermomechanical treatment and coiling temperature on the strengthening mechanisms of low carbon steels microalloyed with Nb. *Materials Science and Engineering: A*, Vol. 685, 2017, pp. 377–390.
[42] Karmakar, A., S. Biswas, S. Mukherjee, D. Chakrabarti, and V. Kumar. Effect of composition and thermo-mechanical processing schedule on the microstructure, precipitation and strengthening of Nb-microalloyed steel. *Materials Science and Engineering: A*, Vol. 690, 2017, pp. 158–169.
[43] Patra, P. K., S. Sam, M. Singhai, S. S. Hazra, G. D. Janaki Ram, and S. R. Bakshi. Effect of coiling temperature on the microstructure and mechanical properties of hot-rolled Ti–Nb microalloyed ultra high strength steel. *Transactions of the Indian Institute of Metals*, Vol. 70, No. 7, 2017, pp. 1773–1781.
[44] Wang, M., F. Zhang, and Z. Yang. Effects of high-temperature deformation and cooling process on the microstructure and mechanical properties of an ultrahigh-strength pearlite steel. *Materials & Design*, Vol. 114, 2017, pp. 102–110.
[45] Zeng, Z., C. Li, Z. Li, Y. Zhai, J. Wang, and Z. Liu. Effect of final cooling temperature on the microstructure and mechanical properties of high-strength anti-seismic rebar. *Materials Research Express*, Vol. 8, No. 9, 2021, id. 96525.
[46] Pereloma, E. V., B. R. Crawford, and P. D. Hodgson. Strain-induced precipitation behaviour in hot rolled strip steel. *Materials Science and Engineering: A*, Vol. 299, No. 1, 2001, pp. 27–37.
[47] Shanmugam, S., R. D. K. Misra, T. Mannering, D. Panda, and S.G. Jansto. Impact toughness and microstructure relationship in niobium- and vanadium-microalloyed steels processed with varied cooling rates to similar yield strength. *Materials Science and Engineering: A*, Vol. 437, No. 2, 2006, pp. 436–445.
[48] Rothleutner, L. M., R. Cryderman, and C. J. Van Tyne. Influence of Temperature and Holding Time on the Interaction of V, Al, and N in Microalloyed Forging Steels. *Metallurgical and Materials Transactions A*, Vol. 45, No. 10, 2014, pp. 4594–4609.
[49] Jiang, B., W. Fang, R. Chen, D. Guo, Y. Huang, C. Zhang, et al. Mechanical properties and microstructural characterization of medium carbon non-quenched and tempered steel: Microalloying behavior. *Materials Science and Engineering: A*, Vol. 748, 2019, pp. 180–188.
[50] Maleki, M., H. Mirzadeh, and M. Zamani. Effect of intercritical annealing time at pearlite dissolution finish temperature (Ac1f) on mechanical properties of low-carbon dual-phase steel. *Journal of Materials Engineering and Performance*, Vol. 28, No. 4, 2019, pp. 2178–2183.
[51] Bilal, N., L. Xiaoyan, L. Yanguo, Y. Zhinan, and Z. Fucheng. Effect of ferrite/martensite on microstructure evolution and mechanical properties of ultrafine vanadium dual-phase steel. *Journal of Materials Engineering and Performance*, 2022.
[52] Chen, S., L. Li, Z. Peng, X. Huo, and J. Gao. Strain-induced precipitation in Ti microalloyed steel by two-stage controlled rolling process. *Journal of Materials Research and Technology*, Vol. 9, No. 6, 2020, pp. 15759–15770.
[53] Gao, J., S. Jiang, H. Zhang, Y. Huang, D. Guan, Y. Xu, et al. Facile route to bulk ultrafine-grain steels for high strength and ductility. *Nature*, Vol. 590, No. 7845, 2021, pp. 262–267.
[54] Zhou, Q., Z. Li, Z. Wei, D. Wu, J. Li, and Z. Shao. Microstructural features and precipitation behavior of Ti, Nb and V microalloyed steel during isothermal processing. *Journal of Iron and Steel Research International*, Vol. 26, No. 1, 2019, pp. 102–111.
[55] Gontijo, M., C. Hoflehner, S. Ilie, J. Six, and C. Sommitsch. Holding time influence on the hot ductility behavior of a continuously cast low alloy steel. *Metals*, Vol. 11, No. 1, 2021, id. 64.
[56] Wang, L., D. Tang, and Y. Song. Prediction of mechanical behavior of ferrite-pearlite steel. *Journal of Iron and Steel Research, International*, Vol. 24, No. 3, 2017, pp. 321–327.
[57] Bu, F.Z., X. M. Wang, L. Chen, S. W. Yang, C. J. Shang, and R. Misra. Influence of cooling rate on the precipitation behavior in Ti-Nb-Mo microalloyed steels during continuous cooling and relationship to strength. *Materials Characterization*, Vol. 102, 2015, pp. 146–155.
[58] Lena, E., F. Jonas, and M. Christian. Local characterization of precipitation and correlation with the prior austenitic microstructure in Nb-Ti-microalloyed steel by SEM and AFM methods. *Metals*, Vol. 8, No. 8, 2018, id. 636.
[59] Li, Z., D. Wen, Y. Ma, Q. Wang, G. Chen, R. Zhang, et al. Prediction of alloy composition and microhardness by random forest in maraging stainless steels based on a cluster formula. *Journal of Iron and Steel Research International*, Vol. 25, No. 7, 2018, pp. 717–723.
[60] Pan, H., H. Ding, and M. Cai. Microstructural evolution and precipitation behavior of the warm-rolled medium Mn steels containing Nb or Nb-Mo during intercritical annealing. *Materials Science and Engineering: A*, Vol. 736, 2018, pp. 375–382.
[61] Zhang, L. C., X. L. Wen, and Y. Z. Liu. Effect of Precipitates on austenite grain growth behavior in a low-carbon Nb-V microalloyed steel. *Materials Science Forum*, Vol. 898, 2017, pp. 783–790.
[62] Yuan, Q., G. Xu, J. Tian, and W. Liang. The recrystallization behavior in ultrafine-grained structure steel fabricated by cold rolling and annealing. *Arabian Journal for Science and Engineering*, Vol. 42, No. 11, 2017, pp. 4771–4777.
[63] Ma, F., G. Wen, and W. Wang. Effect of cooling rates on the second-phase precipitation and proeutectoid phase transformation of a Nb-Ti microalloyed steel slab. *Steel Research International*, Vol. 84, No. 4, 2013, pp. 370–376.
[64] Sun, L., X. Liu, X. Xu, S. Lei, H. Li, and Q. Zhai. Review on niobium application in microalloyed steel. *Journal of Iron and Steel Research International*, Vol. 29, No. 10, 2022, pp. 1513–1525.
[65] Dorin, T., K. Wood, A. Taylor, P. Hodgson, and N. Stanford. Quantitative examination of carbide and sulphide precipitates

in chemically complex steels processed by direct strip casting. *Materials Characterization*, Vol. 112, 2016, pp. 259–268.
[66] Chen, Y., D. Zhang, Y. Liu, H. Li, and D. Xu. Effect of dissolution and precipitation of Nb on the formation of acicular ferrite/bainite ferrite in low-carbon HSLA steels. *Materials Characterization*, Vol. 84, 2013, pp. 232–239.
[67] Wang, X., Y. Zhao, B. Liang, L. Du, and H. Di. Study on isothermal precipitation behavior of nano-scale (Nb,Ti)C in ferrite/bainite in 780 MPa grade ultra-high strength steel. *Steel Research International*, Vol. 84, No. 4, 2013, pp. 402–409.
[68] Jung, J., J. Park, J. Kim, and Y. Lee. Carbide precipitation kinetics in austenite of a Nb–Ti–V microalloyed steel. *Materials Science and Engineering: A*, Vol. 528, No. 16-17, 2011, pp. 5529–5535.
[69] Mao, X., X. Huo, X. Sun, and Y. Chai. Strengthening mechanisms of a new 700MPa hot rolled Ti-microalloyed steel produced by compact strip production. *Journal of Materials Processing Technology*, Vol. 210, No. 12, 2010, pp. 1660–1666.
[70] Hui, Y., H. Pan, N. Zhou, R. Li, W. Li, and K. Liu. Study on strengthening mechanism of 650 MPa grade VN microalloyed automobile beam steel. *Acta Metallurgica Sinica*, Vol. 51, No. 12, 2015, pp. 1481–1488.
[71] Iza-Mendia, A., and I. Gutiérrez. Generalization of the existing relations between microstructure and yield stress from ferrite–pearlite to high strength steels. *Materials Science and Engineering: A*, Vol. 561, 2013, pp. 40–51.
[72] Zhang, D., D. Qiu, M. A. Gibson, Y. Zheng, H. L. Fraser, D. H. Stjohn, et al. Additive manufacturing of ultrafine-grained high-strength titanium alloys. *Nature*, Vol. 576, No. 7785, 2019, pp. 91–95.
[73] Funakawa, Y., T. Shiozaki, K. Tomita, T. Yamamoto, and E. Maeda. Development of high strength hot-rolled sheet steel consisting of ferrite and nanometer-sized carbides. *ISIJ International*, Vol. 44, No. 11, 2004, pp. 1945–1951.
[74] T, G. Precipitation hardening in metals. *Materials Science and Technology*, Vol. 15, No. 1, 1999, pp. 30–36.
[75] Pavlina, E. J., J. G. Speer, and C. J. Van Tyne. Equilibrium solubility products of molybdenum carbide and tungsten carbide in iron. *Scripta Materialia*, Vol. 66, No. 5, 2012, pp. 243–246.
[76] Cao, J. C., X. L. Zhou, L. Deng, Q. L. Yong, X. J. Sun, and Q. Y. Liu. Solubility product of MoC with NaCl type cubic crystal structure in iron. *Advanced Materials Research*, Vol. 476–478, 2012, pp. 281–285.